communications biology

A Nature Portfolio journal

Article

https://doi.org/10.1038/s42003-025-08095-8

Amphiphilic mPEG-PLGA copolymer nanoparticles co-delivering colistin and niclosamide to treat colistin-resistant Gram-negative bacteria infections

Kaifang Yi[1], Xilong Wang[1], Pengliang Li[1], Yanling Gao[2], Dandan He[1], Yushan Pan[1], Xiaoyuan Ma[1], Gongzheng Hu[1] ✉ & Yajun Zhai[1] ✉

Colistin is the last line of defense against multidrug-resistant (MDR) Gram-negative bacterial infections, yet it is restricted due to high drug resistance and toxicity. The combination therapy of colistin and niclosamide exhibits excellent synergistic antibacterial activity against Gram-negative bacteria. How to co-deliver these two drugs with vastly different pharmacokinetic properties in sufficient amounts to the infection site is the core issue that must be resolved for the clinical translation of this drug combination. Here, we designed and prepared a nanosystem capable of co-loading colistin and niclosamide with different physicochemical properties into mPEG-PLGA nanoparticles (COL/NIC-mPEG-PLGA-NPs) to overcome the resistance of multiple colistin-resistant bacteria to colistin and alleviate its toxicity. Mechanistic studies revealed that the COL/NIC-mPEG-PLGA-NPs enhanced the affinity of delivered COL to the modified membrane of colistin-resistant bacteria. The increased membrane permeability caused by colistin promotes an influx of niclosamide, which reduces efflux pump activity and generates intracellular ROS stress, eliminating colistin-resistant bacteria. In addition, the nanoparticles proved non-toxic both in vitro and in vivo. Overall, our study has profound insights into the use of nanosystems with high biosafety for the treatment of infections caused by colistin-resistant bacteria.

Colistin is the last resort antibiotic for the treatment of life-threatening multidrug-resistant (MDR) Gram-negative bacterial infections which are untreatable by other clinically available antibiotics[1,2]. However, since 2015, mobile colistin resistance (*mcr*) genes such as *mcr*-1-10 have spread rapidly around the world, resulting in a great challenge to the antibacterial ability of colistin in recent years[3]. The *mcr* gene leads to modification of colistin target lipid A, resulting in insufficient affinity of colistin to the bacterial membrane[4–6]. The increasing incidence of colistin-resistant bacterial infections, combined with the limited approval of new antibiotics, has led to a global health crisis. Antimicrobial drugs or strategies to reverse colistin resistance are therefore urgently needed to prevent a "post-antibiotic era".

Niclosamide was approved by the US FDA for use in humans to treat tapeworm infection in 1982 and was included in the World Health Organization's list of essential medicines[7]. Niclosamide exhibits antiviral activity against severe acute respiratory syndrome coronavirus and is an effective antibiotic against Gram-positive and acid-fast pathogens (*e.g.*, *Staphylococcus aureus*, *Clostridium difficile*, and *Mycobacterium tuberculosis*), as well as against *Helicobacter pylori*[8]. In the current study, in vitro coadministration of niclosamide and colistin can overcome colistin resistance in Gram-negative bacteria[9,10]. Interestingly, the presence of niclosamide as a therapeutic adjuvant may alleviate concerns about colistin's toxicity to the kidneys[11]. In addition, niclosamide acts as an efflux pump inhibitor to reduce the efflux of colistin, thereby increasing the absorption of niclosamide by bacterial cells and increasing the level of intracellular reactive oxygen species[8]. Therefore, the combination of niclosamide and colistin can achieve synergistic antibacterial effects.

The colistin-niclosamide combination therapy can improve the treatment of colistin-resistant bacterial infections and help eradicate persistent chronic infections[8,10]. The drug combinations can act in parallel to target orthogonal mechanisms and prevent the evolution of resistance pathways. Combination therapy can also work synergistically to enhance a

[1]Henan Agricultural University, Zhengzhou, China. [2]Henan vocational college of Agriculture, Zhengzhou, China. ✉e-mail: yaolilab@126.com; zyj90518@126.com

single pathway, such as improving efficacy by promoting increased absorption of colistin. However, the efficacy of colistin-niclosamide combination therapy for colistin-resistant bacterial infections is still unknown, and drug combinations for treating such infections have not been clinically approved. The common problem with colistin-niclosamide combinations is the drastic difference in pharmacokinetics of colistin and niclosamide, which limits their clinical application[10]. If directly mixed and systemically administered, these two drugs may not be able to reach the infected site at the effective dose to demonstrate synergistic antibacterial activity. On the other hand, toxicity is a matter of concern in the application of colistin. Given its narrow therapeutic window, the plasma colistin concentration required for a therapeutic effect may be in a range that is close to the level at which the drug exhibits nephrotoxicity, and this can vary from one individual to another[12–14]. In addition, whether the combination will further increase the nephrotoxicity and neurotoxicity of colistin is another important issue that has been overlooked. Therefore, appropriate drug delivery systems that can co-deliver colistin and niclosamide without increasing the toxicity of colistin, are required to achieve the reversal of colistin resistance and a synergistic effect in the clinic.

Methoxy poly (ethylene glycol) and poly (D, L-lactide-*co*-glycolide) amphiphilic copolymer (mPEG-PLGA), which is a biodegradable polymer, has been widely used in pharmaceutical and biomedical applications. PLGA is a biocompatible and biodegradable controlled release polymer approved by the FDA for medical applications[15,16]. PLGA can protect loaded drugs from degradation. Sustained release of drug from NPs based on PLGA is likely a result of both the gradual degradation of PLGA and the diffusion of drug through the PLGA matrix[17]. Previous studies have shown that nanoparticles made of PEG-modified PLGA exhibit long-circulation properties in vivo, as the surface of nanoparticles is connected with PEG hydrophilic molecular chains, which cannot be recognized and phagocytized by mononuclear phagocyte system[18,19]. Block copolymers consisting of hydrophobic polyester segments and hydrophilic PEG segments are attracting more and more attention due to their biodegradability, biocompatibility, and customized properties. A variety of drug formulations have been developed using mPEG-PLGA block copolymers, such as injection drug delivery systems, micelles, hydrogels, and nanoparticles[20,21].

In this study, we designed and prepared a nanosystem capable of co-loading two drugs (colistin and niclosamide) with different physicochemical properties into mPEG-PLGA nanoparticles (COL/NIC-mPEG-PLGA-NPs) to overcome the resistance of multiple colistin-resistant bacteria to colistin and alleviate its toxicity. The stability, drug-loading level, and release properties of mPEG-PLGA nanoparticles co-loaded with niclosamide and colistin were evaluated. Antibacterial activity of COL/NIC-mPEG-PLGA-NPs against Gram-negative bacteria *Salmonella* SH05, *Escherichia coli* Y150, and *K. pneumoniae* 5 G in vitro, as well as the therapeutic efficacy in an *E. coli*-induced mouse peritonitis model (systemic infection) were studied (Graphical Abstract).

Results and discussion

COL/NIC-mPEG-PLGA-NPs preparation and optimization

To achieve the co-delivery of colistin and niclosamide, amphiphilic copolymer methoxy poly (ethylene glycol)-poly(lactide-co-glycolide) (mPEG-PLGA) core-shell nanoparticles were prepared using a double emulsification method. We chose mPEG-PLGA as the amphiphilic copolymer model to achieve co-delivery and controlled release of colistin and niclosamide, primarily because PEG and PLGA have been approved by the FDA for clinical use as drug adjuvants. Co-delivery of niclosamide and colistin with distinct solubility and pharmacokinetic properties is not easy to achieve. Due to internal structural separation, the double emulsification method enables amphiphilic copolymers to form nanoparticles capable of encapsulating polar and non-polar cargo, and can improve the controlled release of therapeutic molecules[22]. During the formation of the first emulsification step, hydrophilic colistin was first loaded onto the hydrophilic end of the nanoparticle mPEG to form a hydrophilic nucleus, and then hydrophobic niclosamide dissolved in the mixture of dichloromethane and acetone was added to the hydrophobic end of the nanoparticle PLGA to form a lipophilic layer. The second emulsification step involves using the emulsifying agent PVA to emulsify and produce a W/O/W emulsion. Finally, a core-shell polymer nanoparticle with hydrophilic mPEG as the shell was prepared, in which colistin and niclosamide were co-loaded (Fig. 1a). To the best of our knowledge, the double emulsification method uses a two-step process to prepare a water-in-oil (W/O) emulsion for encapsulating the cargo, which then generates a water-in-oil-in-water (W/O/W) emulsion that uses a combination of surfactants to form nanoparticles[23]. Subsequently, we carried out the optimization of process parameters for the preparation of nanoparticles. In this study, the optimum fitting model was selected using the Design-Expert software. Using the Box–Behnken response surface method, a quadratic regression orthogonal combination test with 3 factors and 3 levels (consisting of 17 test points) was designed, and the optimum polynomial equation was selected by R and P. The relationships among colistin encapsulation efficiency, niclosamide encapsulation efficiency, particle size, and independent variables were elucidated using 3D and contour plots. The model equation is:

$$\begin{aligned} Y_1(\mathrm{NIC-EE}) = &-41.1165 + 36.01625X_1 + 37.3795X + 25.107X_3 \\ &+ 0.505X_1X_2 + 0.32X_1X_3 - 0.66X_2X_3 - 3.53025{X_1}^2 \\ &- 18.081{X_2}^2 - 11.111{X_3}^2 (R^2 = 0.9964, P < 0.0001) \end{aligned}$$

$$\begin{aligned} Y_2(\mathrm{COL-EE}) = &-74.7535 + 45.08X_1 + 31.4505X_2 + 35.8655X_3 \\ &- 0.265X_1X_2 + 0.395X_1X_3 + 0.68X_2X_3 \\ &- 4.4985{X_1}^2 - 13.104{X_2}^2 \\ &- 16.704{X_3}^2 (R^2 = 0.9943, P < 0.0001) \end{aligned}$$

$$\begin{aligned} Y_2(\mathrm{Size}) = &297.225 - 44.375X_1 - 46.3X_2 - 32.05X_3 + 4.5X_1X_2 \\ &+ 2X_1X_3 - 3X_2X_3 + 4.1{X_1}^2 + 15.4{X_2}^2 \\ &+ 14.4{X_3}^2 (R^2 = 0.9626, P < 0.0003) \end{aligned}$$

It could be seen that the model was highly significant (P of the model < 0.0001), with a non-significant $P > 0.05$ for the misfit term. From these results, it can be concluded that this model fits well (Supplementary Tables 1–3). The Box–Behnken response surface method is a multifactor nonlinear experimental optimization method. The fitting equation of this method can predict the value of any test point in the test range very accurately, and therefore has obvious advantages[24]. After optimization of the COL/NIC-mPEG-PLGA-NPs preparation conditions by response surface tests, the optimal preparation conditions were obtained: mPEG-PLGA concentration of 5.04%, dichloromethane to acetone volume ratio of 1:1, and PVA concentration of 1.10% (Fig. 1b–d).

The formulations of COL/NIC mPEG-PLGA-NPs optimized according to the Design Expert software were as follows: the concentration of mPEG-PLGA was 5.04%, the volume ratio of dichloromethane to acetone was 1:1, and the concentration of PVA was 1.10%. The software predicts that the loading capacity (NIC-LC) and encapsulation efficiency (NIC-EE) of niclosamide were 22.04% and 87.88% respectively, while the loading capacity (COL-LC) and encapsulation efficiency (COL-EE) of colistin were 19.77% and 77.56% respectively. Subsequently, COL/NIC mPEG-PLGA-NPs were prepared with the mPEG-PLGA concentration of 5.04%, the volume ratio of dichloromethane to acetone of 1:1, and the PVA concentration of 1.10%. The NIC-EE, NIC-LC, COL-EE, and COL-LC of the prepared COL/NIC-mPEG-PLGA-NPs were 89.03 ± 0.19%, 22.52 ± 0.17%, 77.02 ± 0.49% and 19.48 ± 0.23% respectively. Thus, the optimal preparation method for the COL/NIC-mPEG-PLGA-NPs designed by the Box–Behnken response surface technique was accurate and reliable.

Solid nanoparticle powders with satisfied stability could be stored for a long time. The lyoprotectants were added to the nanoparticles to protect them from stresses and aggregation during the freeze-drying[25]. The type of

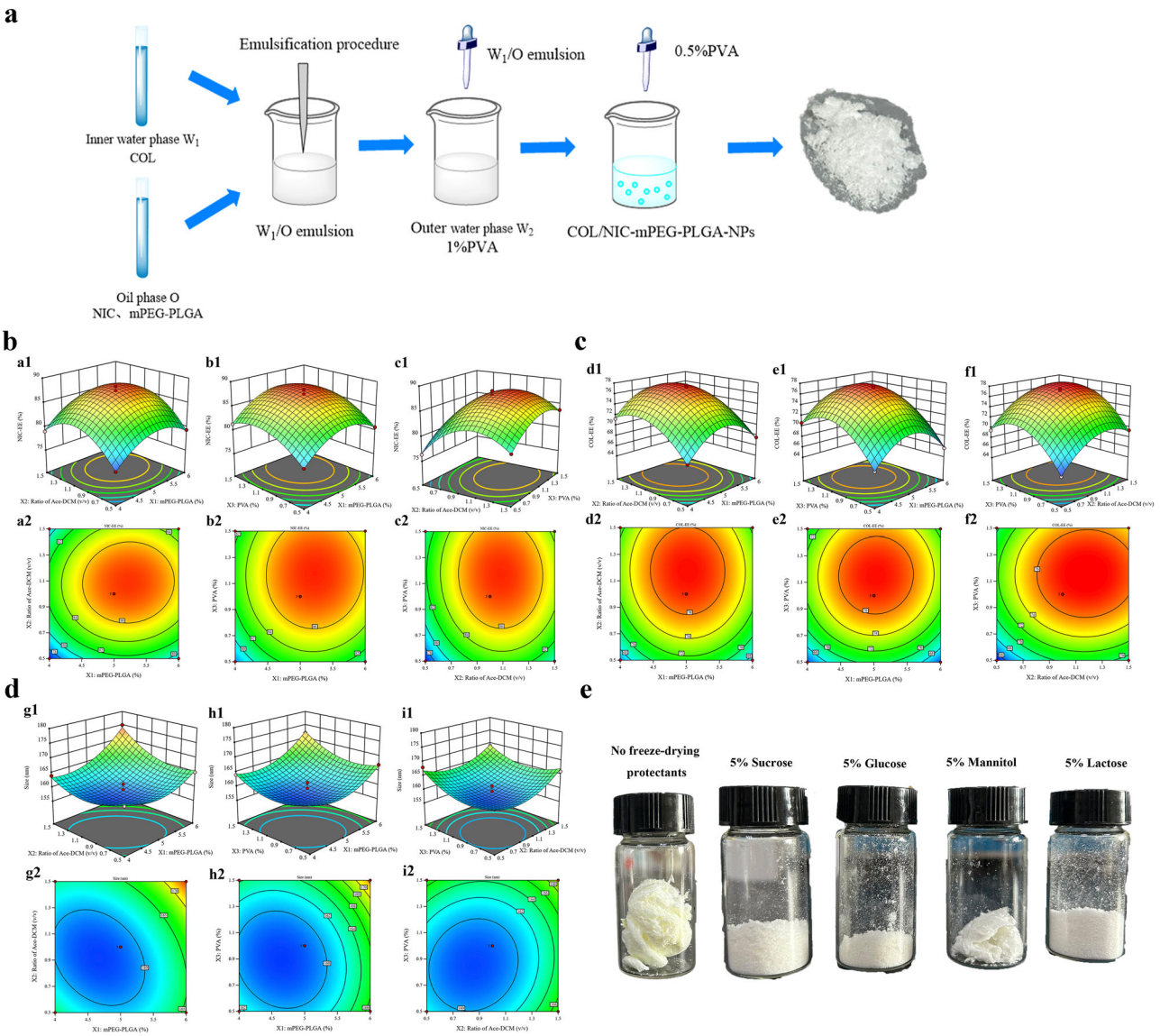

Fig. 1 | Preparation and optimization of COL/NIC-mPEG-PLGA-NPs. **a** Preparation of nanoparticles using the double emulsification method. **b–d** The response surface model demonstrated the influence of mPEG-PLGA concentration, volume ratio of dichloromethane to acetone, and PVA concentration on nanoparticles NIC-EE (**b**), COL-EE (**c**), and size (**d**). **e** Effect of different lyoprotectants on COL/NIC-mPEG-PLGA-NPs.

lyoprotectants affects the particle size and stability of nanoparticles. According to tests on COL/NIC-mPEG-PLGA-NPs treated with different types of cryoprotectants, the results showed that only the sucrose (5%) was complete and uniform, with no significant increase in particle size and polydispersity index (PDI, Fig. 1e and Supplementary Fig. 2). In addition, the shape of sucrose (5%) was relatively regular, and the surface was round and smooth. Therefore, 5% sucrose was suitable as a lyoprotectant for COL/NIC-mPEG-PLGA-NPs.

Characterization of COL/NIC-mPEG-PLGA-NPs

Like other amphiphilic copolymers[26], mPEG-PLGA can be emulsified in aqueous solution to form core-shell nanoparticles. The nanoparticles should be small enough to escape detection and destruction by the reticuloendothelial system, thereby achieving longevity during systemic circulation. Due to the shrinkage of the mPEG shell of polymer nanoparticles, COL/NIC-mPEG-PLGA-NPs were spherical nanoparticles under dry conditions. The average particle size of COL/NIC-mPEG-PLGA-NPs was 170.5 ± 2.23 nm, PDI was 0.265 ± 0.01, zeta potential was −6.44 ± 0.37 mV (Fig. 2a, b). The relatively neutral surface charge (−6.44 ± 0.37 mV) of the PEGylated nanoparticle was advantageous for the stability in a dynamic environment. The neutral surface charge may be beneficial in vivo for systemic administration of drugs to treat bacterial infections, as positively charged surfaces tend to adsorb proteins on the surface, while negatively charged surfaces may not be able to attach to bacterial membranes that also carry negative charges[27]. The morphology of COL/NIC-mPEG-PLGA-NPs was examined by transmission electron microscopy (TEM, Fig. 2c). The images showed that COL/NIC-mPEG-PLGA-NPs were dispersed into single particles with a smooth, round, complete spherical core-shell structure. COL/NIC-mPEG-PLGA-NPs showed a small diameter and polydispersion, which may be attributed to the insertion of hydrophobic drugs that allow the amphiphilic copolymers to form a well-knit structure. In addition, fourier transform infrared (FTIR) results showed that in the COL spectrum, the characteristic amido-carbonyl peak of colistin appeared at 1657.36 cm^{-1}. In the NIC spectrum, the peak of phenolic hydroxyl group appeared at 3577.16 cm^{-1}, the stretching vibration peak of C-H on the benzene ring was at 3095.67 cm^{-1}, and 1652.80 cm^{-1} represented C = O on amide group. In the spectrum of mPEG-PLGA, the characteristic peak of mPEG-PLGA was seen at 1746.14 and 1080.30 cm^{-1}. In the spectrum of

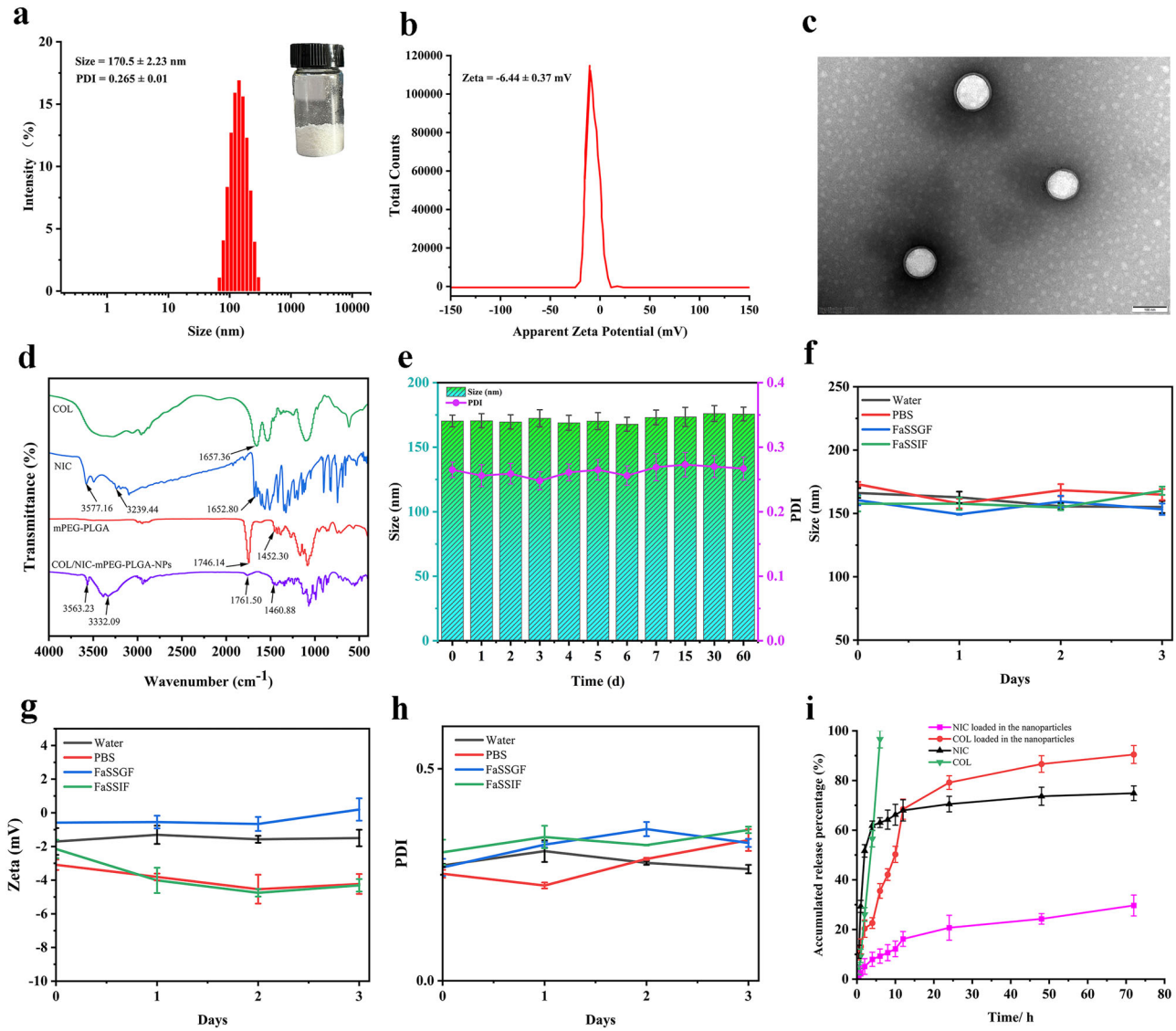

Fig. 2 | Characterization of COL/NIC-mPEG-PLGA-NPs. a Particle size and size distribution of COL/NIC-mPEG-PLGA-NPs. **b** Zeta potential characterization of COL/NIC-mPEG-PLGA-NPs. **c** Representative TEM image of COL/NIC-mPEG-PLGA-NPs. **d** FTIR spectra of colistin, niclosamide, mPEG-PLGA, COL/NIC-mPEG-PLGA-NPs. **e** Storage stability of COL/NIC-mPEG-PLGA-NPs at 4 °C. **f–h** Changes in the size (**f**), Zeta (**g**), and PDI (**h**) of COL/NIC-mPEG-PLGA-NPs stored in various media at 37 °C for 3 days. (PBS phosphate-buffered saline, FaSSGF fasted state simulated gastric fluid, FaSSIF fasted state simulated intestinal fluid, $n = 3$). **i** The colistin and niclosamide release profile of COL/NIC-mPEG-PLGA-NPs. The experiments were repeated three times independently, and representative data are displayed.

COL/NIC-mPEG-PLGA-NPs (Fig. 2d), the characteristic absorption peaks of COL, NIC and mPEG-PLGA seemed not to change much, indicating that the basic skeleton of nanoparticle did not change greatly. These results indicate that colistin and niclosamide are successfully loaded into nanoparticles formed from mPEG-PLGA polymers.

In consideration of the potential utility of co-delivery of COL/NIC-mPEG-PLGA-NPs, stability is important for long-term storage and scalable processing. As shown in the results of Fig. 2e, after being stored at 4 °C for 2 months, the color, shape, particle size, and PDI of the freeze-dried powder product did not change, and this stable character made the NPs show significant potential in clinical implications. Moreover, the size, PDI, and Zeta potential of COL/NIC-mPEG-PLGA-NPs dispersed under different aqueous conditions remained stable, including water, phosphate-buffered saline (PBS), fasted state simulated gastric fluid (FaSSGF) and intestinal fluid (FaSSIF), and no significant aggregates were observed over 3 days (Fig. 2f–h). The COL and NIC release profile of COL/NIC-mPEG-PLGA-NPs fitted the first-order kinetic equation: $Q = 89.54(1\text{-}e^{-0.09t})$ ($R^2 = 0.9715$, for COL) and $Q = 27.64(1\text{-}e^{-0.07t})$ ($R^2 = 0.9734$, for NIC), respectively. Compared with nonencapsulated drugs, the drug release from the nanoparticles had a pronounced prolongation (Fig. 2i, Supplementary Fig. 3 and Supplementary Table 5). The mPEG-modified PLGA could help the nanoparticles escape from reticuloendothelial system phagocytosis and prolong their circulation in the bloodstream[18,19]. Our results found that the nanoparticles can remain stable in different media, suggesting that the superior stability of PEGylated nanoparticles, especially in simulated gastrointestinal fluids, can provide extended blood circulation, which is ideal for the treatment of bacterial infections.

Antibacterial activity of the COL/NIC-mPEG-PLGA-NPs against colistin-resistant bacteria in vitro

To evaluate the antibacterial efficacy of the COL/NIC-mPEG-PLGA-NPs, MIC and time-kill curve were first assessed against the colistin-resistant Gram-negative bacteria (*mcr*-1 positive). After 24 h of treatment, COL/NIC-mPEG-PLGA-NPs (128 μg/mL) containing colistin and niclosamide at 1.25 and 0.48 μg/mL, respectively, showed excellent antibacterial activity against colistin-resistant clinical strains with over 3-log reduction compared

to the blank group or monotreatment for all the tested colistin-resistant strains (Fig. 3a–c and Supplementary Table 6). However, the free drug combinations (colistin and niclosamide) at the same concentration as that of COL/NIC-mPEG-PLGA-NPs showed no obvious antibacterial activity (Fig. 3d–f). These results demonstrated that colistin and niclosamide are encapsulated in nanoparticles with slow-release properties, which allows COL/NIC-mPEG-PLGA-NPs to overcome the colistin-resistant and provide long-lasting antibacterial effects. The enhanced antibacterial activity of COL/NIC-mPEG-PLGA-NPs was further confirmed by live/dead bacterial staining and scanning electron microscopy (SEM) examination of bacterial surface morphology. Live/dead staining further demonstrated that the treatment with COL/NIC-mPEG-PLGA-NPs caused significant damage of the bacterial membrane, leading to bacterial lysis (Fig. 3g). SEM images showed rough bacterial surfaces or lysed bacterial cells that have been destroyed and damaged by COL/NIC-mPEG-PLGA-NPs treatment (Fig. 3h). Thus, COL/NIC-mPEG-PLGA-NPs delivered both drugs effectively without sacrificing drug potency and enhanced the inhibition of colistin-resistant Gram-negative bacteria growth when compared to colistin or niclosamide treatments alone.

Antibacterial mechanism of COL/NIC-mPEG-PLGA-NPs

To understand the mechanism for resistance reversal of COL/NIC-mPEG-PLGA-NPs, the mode of action was explored using the *mcr*-1-carrying *E. coli Y*150 strain as an example. As shown in Fig. 3h, COL/NIC-mPEG-PLGA-NPs attached to the surface of colistin-resistant bacteria during the four hours of incubation followed by bacterial membrane disruption. Considering the effective adhesion of COL/NIC-mPEG-PLGA-NPs to the membrane, we hypothesized that the formation of the particles might enhance the affinity of COL to the colistin-resistant bacterial membrane. In *mcr*-1 positive strains, the outermost layer of the membrane lipopolysaccharide has been modified by MCR-1 protein, which makes it difficult for COL alone to interact with the membrane[4]. As expected, we found that the higher uptake of COL/NIC-mPEG-PLGA-NPs resulted in significantly increased membrane permeability, which was revealed by the fluorescent analysis of the NPN probe (Fig. 4a). In addition, COL/NIC-mPEG-PLGA-NPs and Blank-NPs exhibited higher fluorescence intensity than free COL, as mPEG modified PLGA can increase the permeability of bacterial cell membranes[28]. The increase in membrane permeability usually causes the dissipation of the membrane potential. So, we investigated the membrane potential of the cells treated with COL/NIC-mPEG-PLGA-NPs using the potential-sensitive membrane dye $DiSC_3(5)$ (Fig. 4b). The increase in fluorescence signal after COL/NIC-mPEG-PLGA-NPs treatment indicates membrane depolarization and membrane potential dissipation. This indicates that COL/NIC-mPEG-PLGA-NPs can affect bacterial PMF by affecting the dissipation of membrane potential. Thus, the increased permeability of COL/NIC-mPEG-PLGA-NPs treatment indicates that the formulation has successfully restored the antibacterial activity of COL to colistin-resistant bacteria, and the enhanced interaction between COL and bacterial membrane may be due to the polymer mPEG-PLGA's ability to adhere to the surface of bacteria and interact more easily with the bacterial outer membrane.

Secondly, niclosamide can be used as an efflux pump inhibitor to overcome the resistance of *E. coli*, promote the intracellular retention of colistin, and enhance its antibacterial activity[8]. Compared with the control group without any treatment, the fluorescence intensity of free niclosamide increased, indicating that niclosamide had an inhibitory effect on the EtBr efflux pump. More importantly, nanoparticles containing both colistin and niclosamide displayed the highest fluorescence intensity in colistin-resistant *E. coli* when compared with niclosamide treated bacteria, demonstrating that the enhanced uptake of niclosamide in the nanoparticles combination treatment could lead to more efficient binding of niclosamide to the efflux pump, resulting in reduced efflux of EtBr in bacteria (Fig. 4c).

Next, we measured intracellular ATP levels, since ATP production is the process most associated with membrane potential, which depends on the PMF produced by the electron transport chain. We found that after treatment with COL/NIC-mPEG-PLGA-NPs, intracellular ATP levels decreased rapidly, which was consistent with the dissipation of PMF (Fig. 4d). The inhibition of electron transport and oxidative phosphorylation processes is also involved in intracellular ROS accumulation, which is associated with bacterial death. Thus, we monitored the intracellular ROS level of bacteria upon COL/NIC-mPEG-PLGA-NPs treatment and found that the intracellular ROS levels increased significantly (Fig. 4e). To confirm the contribution of ROS stress to the potent bactericidal capacity of COL/NIC-mPEG-PLGA-NPs, the antimicrobial performance of COL/NIC-mPEG-PLGA-NPs was evaluated in the presence of the commonly used ROS quencher L-ascorbic acid (L-Aa, 10 mM). Although COL/NIC-mPEG-PLGA-NPs still showed bacterial reduction, the presence of L-Aa significantly reduced the antibacterial activity of COL/NIC-mPEG-PLGA-NPs (Fig. 4f and Supplementary Fig. 4). This finding demonstrated the vital role of ROS stress in the antibacterial activity of the nanoparticles. ROS, mainly including three types, superoxide anions ($O_2\bullet^-$), hydrogen peroxide (H_2O_2), and hydroxyl radicals (•OH), play an important role in the bactericidal processes of antibiotics[29,30]. Interestingly, we also found that COL/NIC-mPEG-PLGA-NPs treatment significantly promoted the production of H_2O_2 (Fig. 4g). Thus, COL/NIC-mPEG-PLGA-NPs trigger ROS accumulation, which correspondingly increases membrane damage and further reduces bacterial activity. These results indicate that COL/NIC-mPEG-PLGA-NPs can dissipate PMF, reduce ATP production, and increase oxidative stress, leading to cell death.

In summary, the antibacterial activity of mPEG-PLGA copolymer nanoparticles co-loaded with COL and NIC can be divided into three steps: (1) COL/NIC-mPEG-PLGA-NPs interact with bacterial membranes via mPEG-PLGA, causing an increase in membrane permeability and dissipation of membrane potential; (2) COL/NIC-mPEG-PLGA-NPs release COL to disrupt bacterial membranes, alter membrane permeability, and disrupt membrane integrity; (3) the leaky membrane allows more COL and NIC to flow into the bacterial cytoplasm, and NIC inhibits efflux pump activity to effectively reduce the efflux of internalized drugs, resulting in reduced ATP production and elevated ROS stress, ultimately leading to killing of resistant pathogens.

Biocompatibilities of COL/NIC-mPEG-PLGA-NPs in vitro and in vivo

Although it has been reported that colistin, niclosamide, and polymer mPEG-PLGA all have good biocompatibility, it is necessary to evaluate the in vitro and in vivo biocompatibility of COL/NIC-mPEG-PLGA-NPs[11,16,31]. We evaluated the blood biocompatibility of COL/NIC-mPEG-PLGA-NPs through a hemolysis test. The hemolysis results showed that mouse red blood cells treated with different concentrations of COL/NIC-mPEG-PLGA-NPs did not show hemolysis, with a hemolysis level < 1%, indicating that COL/NIC-mPEG-PLGA-NPs had broad safety in direct or indirect blood contact applications (Fig. 5a). Cell viability analysis using cell counting kit-8 (CCK-8) showed that COL/NIC-mPEG-PLGA-NPs neither exerted cytotoxicity toward PK-15 cells at an effective antibacterial concentration (64 μg/mL) nor damaged them at a concentration as high as 1000 μg/mL (Fig. 5b). Furthermore, at the effective doses, there were no significant differences in the viability of RAW 264.7 cells among different dose groups, indicating that the cytotoxicity of COL/NIC-mPEG-PLGA-NPs was negligible (Supplementary Fig. 5).

Nephrotoxicity is a concern with colistin use, which limits its clinical use. Interestingly, it has been reported that niclosamide acts as an intervention in the event of kidney damage. Treatment with niclosamide dramatically improved renal function in a rat model of renal ischemia/reperfusion injury as evidenced by low levels of biomarkers for kidney damage compared to the control[11]. As shown in Fig. 5c–f, compared with the colistin group, the levels of alanine aminotransferase (ALT), aspartate aminotransferase (AST), urea nitrogen (BUN), and creatinine (CREA) in the COL/NIC-mPEG-PLGA-NPs (L) and COL/NIC-mPEG-

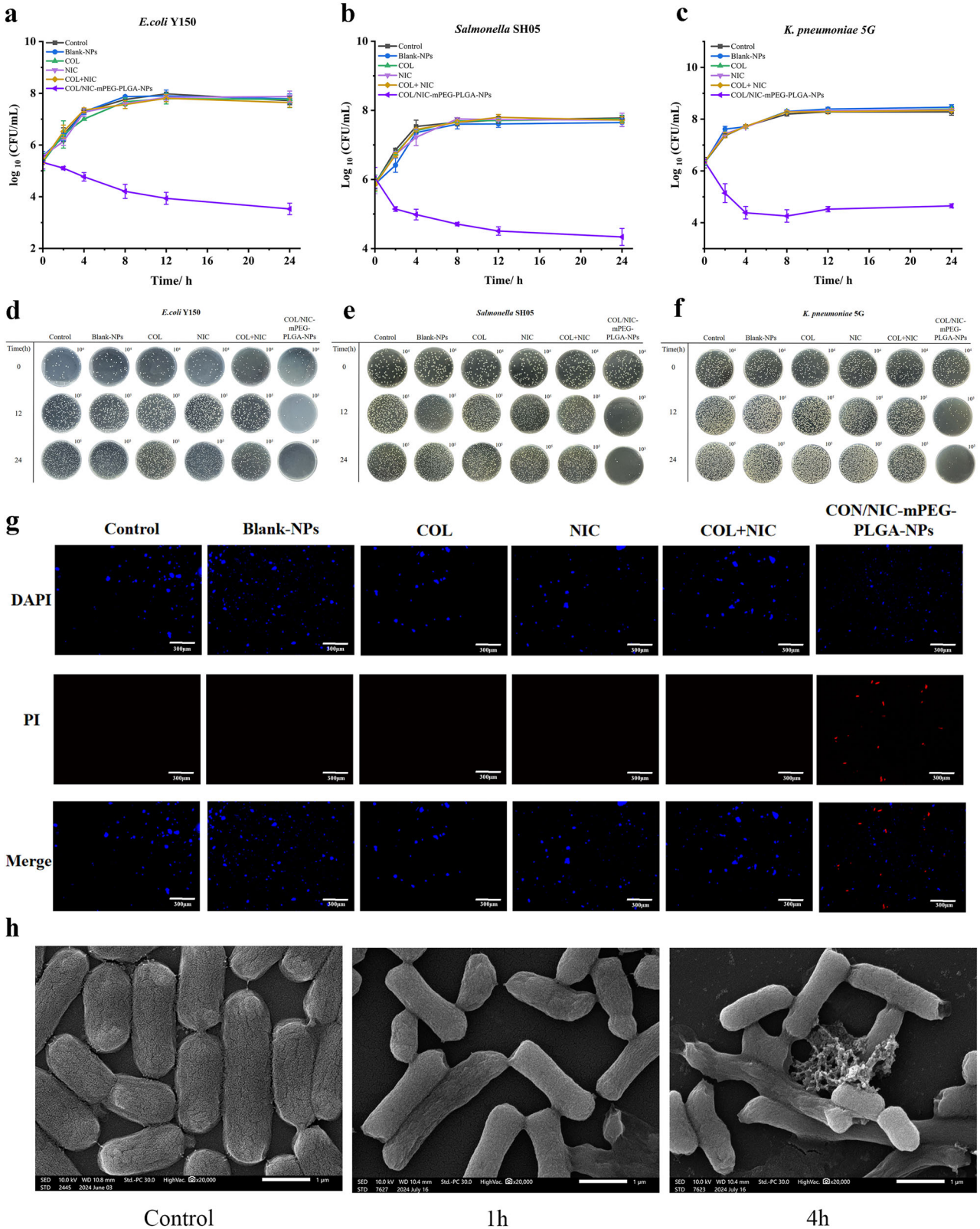

Fig. 3 | Antibacterial activity of COL/NIC-mPEG-PLGA-NPs in vitro. **a**–**c** Time–kill curves of colistin-resistant Gram-negative bacteria (*mcr*-1 positive) *Salmonella* SH05 (**a**), *E. coli* Y150 (**b**) and *K. pneumoniae* 5 G (**c**) treated with various formulations (COL colistin 1.25 μg/mL; NIC niclosamide 0.48 μg/mL; Blank-NPs blank nanoparticles 128 μg/mL; COL/NIC-mPEG-PLGA-NPs: nanoparticles 128 μg/mL containing colistin at 1.25 μg/mL and niclosamide at 0.48 μg/mL). **d**–**f** Colony images of colistin-resistant *Salmonella* SH05 (**d**), *E. coli* Y150 (**e**), and *K. pneumoniae* 5 G (**f**) treated with various formulations for 24 h at 37 °C. **g** Confocal fluorescent images of live and dead bacterial cells after incubation with various formulations for 2.5 h. Blue fluorescence shows bacterial quasi-nuclear stained with DAPI, while red fluorescence shows dead bacteria stained with PI. The scale bar is 300 μm. **h** Scanning electron microscopic (SEM) images of *mcr*-1-carrying *E. coli* Y150 after COL/NIC-mPEG-PLGA-NPs treatment for 1 or 4 h. All the growth curves and bactericidal test were determined in triplicate, and representative data are displayed.

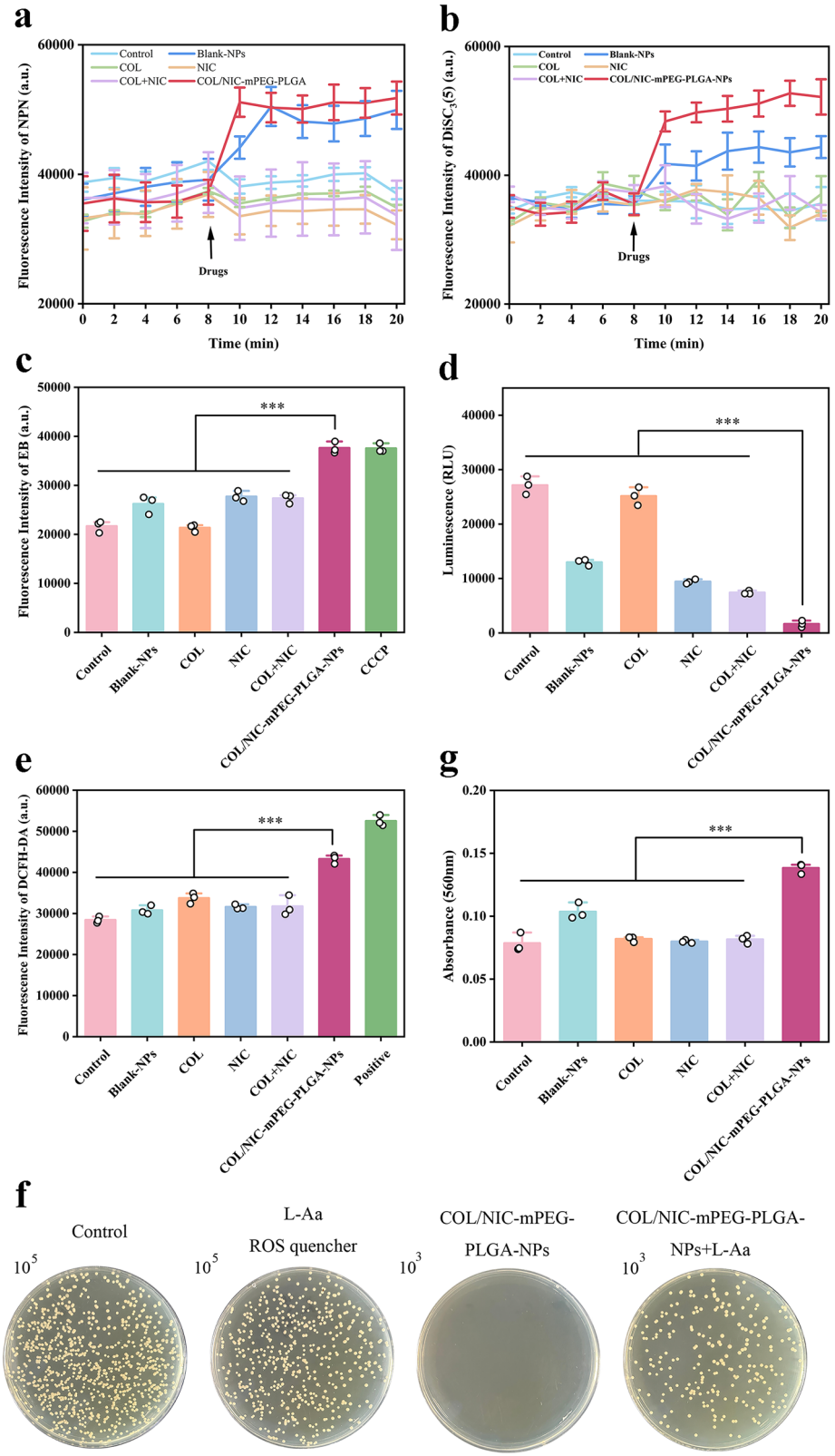

Fig. 4 | Antibacterial mechanisms of COL/NIC-mPEG-PLGA-NPs against colistin-resistant *E. coli*. **a** Membrane permeability analysis of bacteria treated with PBS, COL (1.25 μg/mL), NIC (0.48 μg/mL), COL + NIC (1.25 μg/mL + 0.48 μg/mL), Blank-NPs (128 μg/ mL), or COL/NIC-mPEG-PLGA-NPs (nanoparticles 128 μg/mL containing colistin at 1.25 μg/mL and niclosamide at 0.48 μg/mL) via fluorescence of NPN. **b** $DiSC_3(5)$ membrane potential measurement for different treatments. **c** Ethidium bromide (EtBr) accumulation in different treatments (CCCP, positive control) after 1 h to reflect the efflux pump effect. **d** Intracellular ATP levels at different treatments. **e** Intracellular ROS generation profile of bacteria after different treatments for 30 min via the ROS probe DCFH-DA. **f** Plate colony images of bacteria treated with COL/NIC-mPEG-PLGA-NPs in the presence or absence of ROS quencher L-ascorbic acid (L-Aa, 10 mM). **g** H_2O_2 levels at different treatments. ($n = 3$; $^{***}p < 0.001$, $^{**}p < 0.01$; analysis performed using one-way ANOVA with Tukey's post-hoc test).

PLGA-NPs (M) treatment groups were significantly reduced ($p < 0.001$), indicating that COL/NIC-mPEG-PLGA-NPs can alleviate liver and kidney damage in mice within a certain concentration range. Encapsulating COL in COL/NIC-mPEG-PLGA-NPs can reduce its nephrotoxicity. Thus, COL/NIC-mPEG-PLGA-NPs exhibit excellent biocompatibility in vitro and in vivo.

In vivo real-time tracking

We evaluated the in vivo distribution of COL/NIC-mPEG-PLGA-NPs by using an optical imaging system. Mice were intravenously injected with COL/NIC-mPEG-PLGA-NPs loaded with DiR (denoted as DiR-COL/NIC-mPEG-PLGA-NPs), and were monitored using an in vivo imaging system (IVIS). The DiR signal was observed in the liver and spleen within 3 h

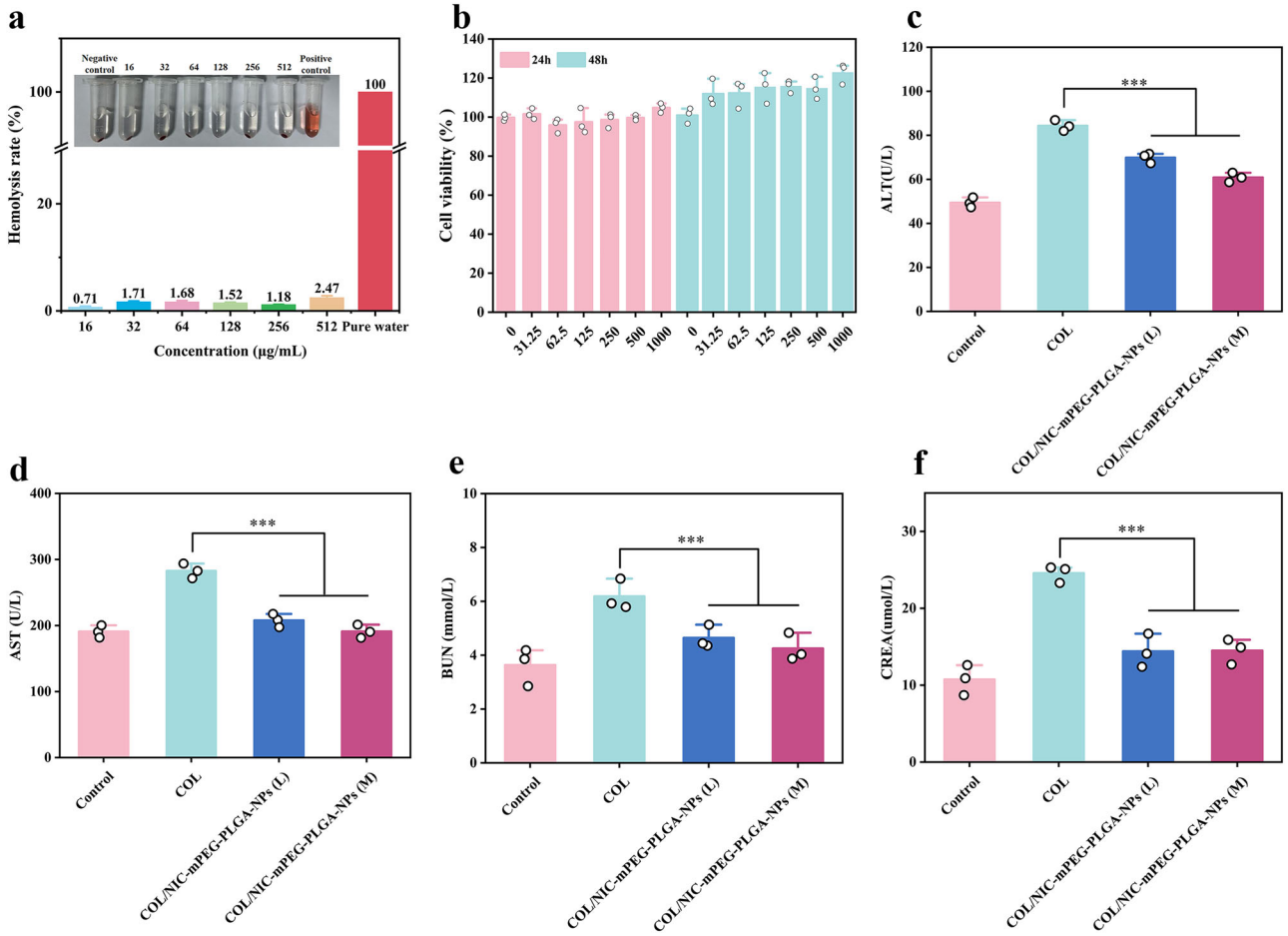

Fig. 5 | In vitro and in vivo biocompatibility of the COL/NIC-mPEG-PLGA-NPs. **a** Hemolysis assay and quantification of red blood cells (RBCs) incubated with COL/NIC-mPEG-PLGA-NPs at different concentrations for 1 h. **b** Viability of porcine kidney-15 (PK-15) cells after treatment with different concentrations of COL/NIC-mPEG-PLGA-NPs for 24 h and 48 h. **c–f** Liver and renal function-related indices (ALT, AST, BUN, and CREA) of mice after treatment with low (20 mg/kg) and high (40 mg/kg) doses of COL/NIC-mPEG-PLGA-NPs. ($n = 3$; $^{***}p < 0.001$; analysis performed using one-way ANOVA with Tukey's post-hoc test).

and enhanced after 6 h of treatment, while very weak signals were observed in other organs (Supplementary Fig. 6).

Additionally, the time-dependent biodistribution and targeting efficiency of COL/NIC-mPEG-PLGA-NPs containing near-infrared dye DiR were evaluated in a mouse thigh infection model using an optical imaging system. As shown in Fig. 6a, PBS (100 μL) and *E. coli* Y150 (1.2×10^8 CFU/mouse, 100 μL) were injected into the left thigh and the right thigh respectively (i.e., the uninfected site and the infected site). After 24 h, we intravenously injected DiR-labeled nanoparticles (referred to as DiR-COL/NIC-mPEG-PLGA-NPs) and monitored their distribution using IVIS. As shown in Fig. 6b, DiR-COL/NIC-mPEG-PLGA-NPs demonstrated effective targeting to the inflamed tissue and had a relatively long residence time within it. Compared with the uninfected sites, the fluorescence signals at the infected sites gradually increased over time and finally reached their strongest intensity at 24 h (Fig. 6b, d). The major organs and tissues were collected for imaging 24 h after treatment. The in vitro biodistribution data showed that DiR-COL/NIC-mPEG-PLGA-NPs were mainly distributed in the liver, spleen, and the infected site (Fig. 6c, e). The fluorescence intensity at the infected site was significantly higher than that at the uninfected site, indicating that COL/NIC-mPEG-PLGA-NPs can be retained at the *E. coli*-infected site through targeting properties. Intense fluorescence signals were observed in the liver and spleen, indicating that the nanoparticles underwent normal metabolic pathways in vivo. Our results indicate that COL/NIC-mPEG-PLGA-NPs possess targeting properties and can effectively locate and be retained at the sites of bacterial infections, providing valuable insights into their site-specific delivery capabilities in combating infections caused by colistin-resistant bacteria.

Antibacterial activity of the mPEG-PLGA polymer nanoparticles co-drug delivery system in vivo

The antibacterial efficacy of COL/NIC-mPEG-PLGA-NPs in vivo was investigated in a mouse peritonitis-sepsis infection model. Mice were infected by clinically isolated colistin-resistant MDR *E. coli* by intraperitoneal injection. COL, NIC, COL + NIC, or COL/NIC-mPEG-PLGA-NPs (low, medium, and high dose group) were intraperitoneally administrated at 1 h postinfection, and the saline-treated group was used as the negative control (Fig. 7a). As shown in Fig. 7b, infected mice treated with COL/NIC-mPEG-PLGA-NPs showed a higher survival rate (50% for COL/NIC-mPEG-PLGA-NPs-L, 75% for COL/NIC-mPEG-PLGA-NPs-M, and 37.5% for COL/NIC-mPEG-PLGA-NPs-H). The mortality rate of mice treated with free COL or NIC was approximately 60%, indicating limited therapeutic efficacy of the monotherapy (Fig. 7b). In contrast, the COL/NIC-mPEG-PLGA-NPs-M treatment showed greatly improved therapeutic efficacy against peritonitis-sepsis, which was evidenced by 75% survival rate of the infected mice, significantly higher than that of control infected mice (survival rate: 0%) and mice treated with combination therapy (survival rate: 50%). In addition, throughout the treatment period, the weight of the mice gradually recovered and slightly increased with the treatment of COL/NIC-mPEG-PLGA-NPs (Fig. 7c).

In order to investigate whether the improved survival rate of infected mice was due to the potent antibacterial activity of COL/

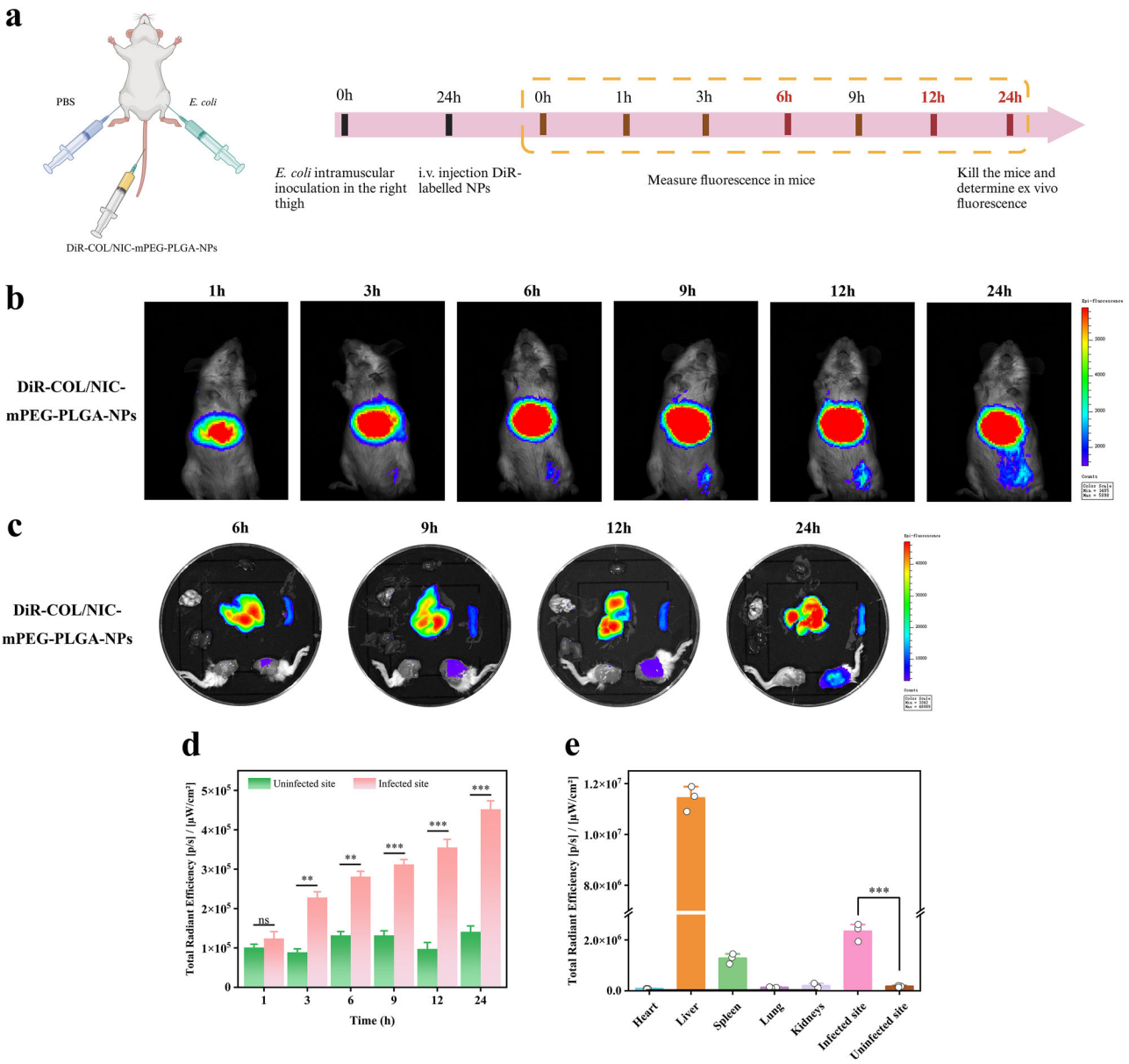

Fig. 6 | The targeting efficiency of COL/NIC-mPEG-PLGA-NPs in mice infected with *E. coli*. **a** Schematic diagram of the infection model. *E. coli* Y150 was injected into the right thigh muscle of mice, denoted as the infected site. PBS was injected into the left thigh muscle, denoted as the uninfected site. DiR-labeled COL/NIC-mPEG-PLGA-NPs were administered via intravenous injection. **b** The representative fluorescence images of the infected mice at different time intervals. **c** Fluorescence images of the major organs and tissues collected from mice infected with *E. coli* 24 h after treatment with nanoparticles. These organs and tissues are labeled as follows: heart (H), liver (Li), spleen (S), lung (Lu), kidney (K), infected site (I), and uninfected site (U). **d** Fluorescence quantitative analysis of the infected site and the uninfected site. Statistical analysis was performed on the infected site group and the uninfected site group, with $n = 3$. **e** Fluorescence quantitative analysis of organs or tissues in vitro images ($n = 3$). $^{**}p < 0.01$, $^{***}p < 0.001$, and ns $p > 0.05$, respectively.

NIC-mPEG-PLGA-NPs, we counted the bacterial colony forming units (CFUs) in ascites and major organs of the infected mice exposed to different therapies after 24 h of bacterial infection. Comparing the number of bacteria present in the various tissues and organs of the infected mice, there was almost no bacterial reduction in the COL or NIC group, while the counts of bacteria in the peritoneal fluid, liver, spleen, and kidney of the COL/NIC-mPEG-PLGA-NPs groups were significantly reduced with approximately 2-log to 4-log reduction of bacterial CFU, suggesting that COL/NIC-mPEG-PLGA-NPs could prevent potential failure of organs caused by bacterial infection (Fig. 7d–g).

Inflammation analysis was further conducted to study if COL/NIC-mPEG-PLGA-NPs treatment is superior to monotreatment with the free antibiotic COL or adjuvant NIC. Importantly, compared to the infected mice without treatment or those treated with NIC, COL, or COL + NIC (niclosamide plus colistin), the levels of proinflammatory cytokines such as IL-6 (Fig. 7h), IL-1β (Fig. 7i), and TNF-α (Fig. 7j) were significantly reduced in the mice following COL/NIC-mPEG-PLGA-NPs treatment. Hematoxylin and eosin (H&E) staining also revealed that the infection of *mcr*-positive *E. coli* Y150 resulted in severe inflammatory response, and a large number of neutrophils (marked by black arrows) were observed in untreated mice. Similarly, neither free COL nor NIC treatment yielded any alleviation of neutrophil infiltration, indicating that their therapeutic effect was limited at the test dose, consistent with their weaker ability to clear bacterial load mentioned above. However, mice treated with COL/NIC-mPEG-PLGA-NPs showed a significant decrease in the number of inflammatory cells, indicating effective relief of inflammatory symptoms (Fig. 7k). Moreover, histopathological

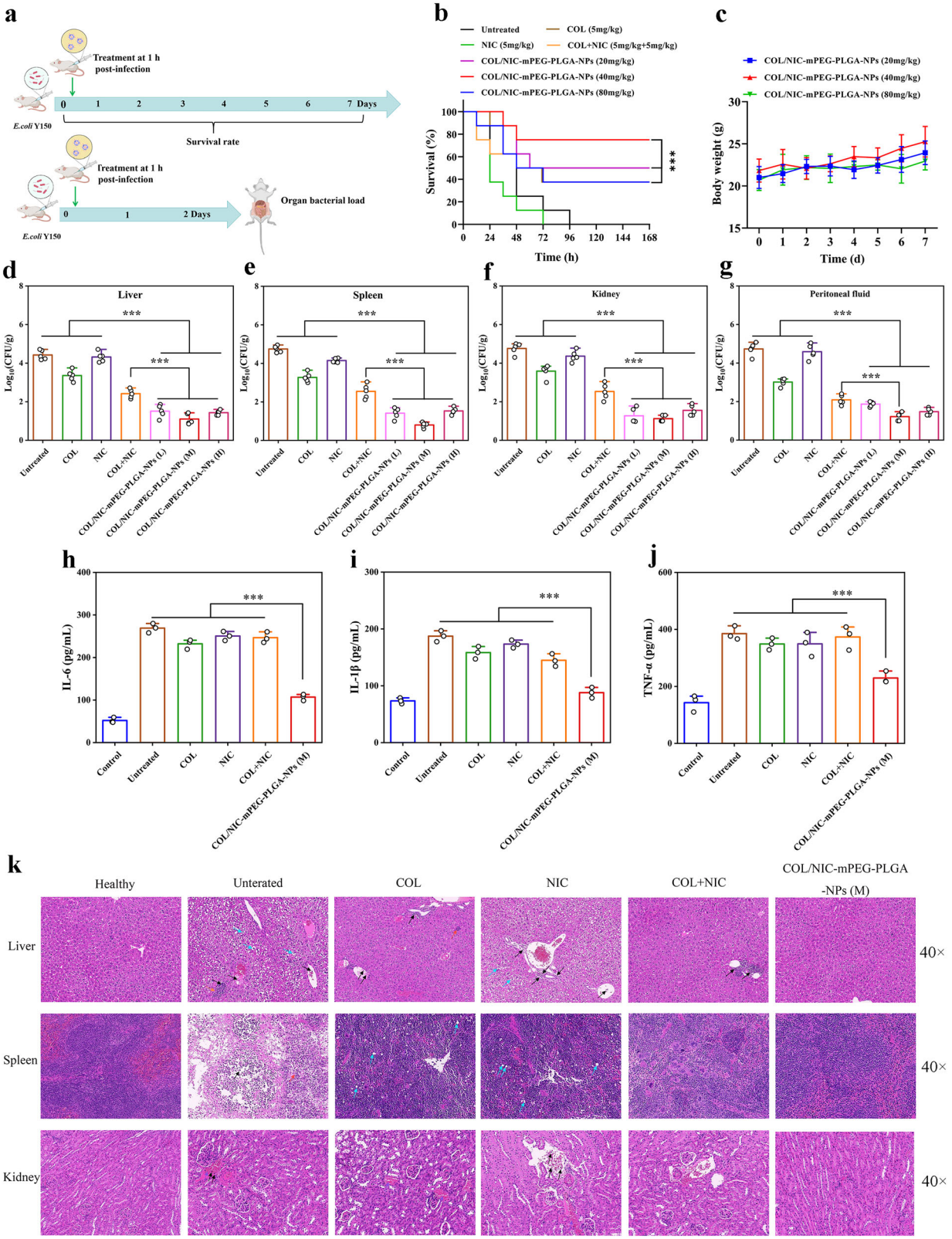

analysis showed that treatment with COL/NIC-mPEG-PLGA-NPs alleviated tissue injury induced by *E. coli* infection, including hepatocyte inflammatory cell infiltration, splenic damage, and glomerular vacuoles (Fig. 7k). Together, these studies indicate that COL/NIC-mPEG-PLGA-NPs therapy is the most effective treatment method for reducing bacterial burden, physiological markers of infection and inflammation, and improving overall survival outcomes.

Conclusions

In this study, we designed and prepared a nanosystem capable of co-loading two drugs (colistin and niclosamide) with different physicochemical properties into mPEG-PLGA nanoparticles (COL/NIC-mPEG-PLGA-NPs) to overcome the resistance of multiple colistin- resistant bacteria to colistin and alleviate its toxicity. This nanosystem successfully reversed colistin resistance in clinically isolated colistin-resistant bacteria by

Fig. 7 | Therapeutic efficacy of COL/NIC-mPEG-PLGA-NPs in a mouse peritonitis-sepsis infection model induced by colistin-resistant *E. coli*. **a** Schematics of establishment of the peritonitis-sepsis mouse model and treatment schedule. Mice were infected with clinically isolated colistin-resistant *E. coli* Y150 isolate (1.5×10^8 CFU) via intraperitoneal injection followed by intraperitoneal injection of COL (5 mg/kg), NIC (5 mg/kg), COL + NIC (5 mg/kg), COL/NIC-mPEG-PLGA-NPs (L) (20 mg/kg), COL/NIC-mPEG-PLGA-NPs (M) (40 mg/kg), or COL/NIC-mPEG-PLGA-NPs (H) (80 mg/kg) at 1 h postinfection. **b** The Survival rate of infected mice after different treatments ($n = 8$). **c** Body weight changes during the treatment by COL/NIC-mPEG-PLGA-NPs (20 mg/kg, 40 mg/kg, and 80 mg/kg) after *E. coli Y150* infection are plotted. **d**–**g** Quantification of the number of bacteria in the liver (**d**), spleen (**e**), kidney (**f**), and peritoneal fluid (**g**) of the infected mice with different treatments. Infected mice without any treatment were used as controls ($n = 5$). Serum levels of IL-6 (**h**), IL-1β (**i**), and TNF-α (**j**) measured via enzyme-linked immunosorbent assay (ELISA; $n = 3$). **k** Histomorphology of the liver, spleen, and kidney in mice after different treatments. Scale bar: 50 μm. Black arrows indicate inflammatory cell infiltration. Orange arrows indicate cell necrosis. Blue arrows indicate vacuolation. Purple arrows indicate fluid congestion. (***$p < 0.001$; analysis performed using one-way ANOVA with Tukey's post-hoc test).

enhancing the affinity of colistin to the bacterial membrane and improving the colistin and niclosamide uptake by the bacteria to generate lethal ROS. More importantly, a colistin-resistant mouse peritonitis-sepsis infection model demonstrated the excellent therapeutic efficacy of COL/NIC-mPEG-PLGA-NPs. In addition, the nanoparticles proved non-toxic both in vitro and in vivo. Taken together, our therapeutic mPEG-PLGA nanoparticle system has great potential to specifically co-deliver colistin and niclosamide to inflammatory tissues and bacteria to treat bacterial infections effectively.

Materials and methods

Materials

The *mcr*-1 positive colistin-resistant bacteria including *Salmonella Typhimurium* (*Salmonella* SH05, *Salmonella* 2a), *E. coli* (*E. coli* Y150, *E. coli* E31), and *K. pneumoniae* (*K. pneumoniae* 5G, *K. pneumoniae* 3Q) were clinically colistin-resistant isolates identified and preserved by our laboratory. Enhanced ATP Assay Kit, ROS Assay Kit, and Hydrogen Peroxide Assay Kit were obtained from Beyotime Biotechnology, Shanghai, China. 1-N-phenylnaphthylamine (NPN), 3,3-Dipropylthiadicarbocyanine iodide $DiSC_3(5)$, 4′-6-diamidino-2-phenylindole (DAPI), propidium iodide (PI), and EtBr were obtained from Sigma-Aldrich (Shanghai, China). Monomethoxy (polyethylene glycol)—poly (D, L-lactide-*co*-glycolide) (mPEG-PLGA) (mPEG5000-PLGA3000, 75:25) was obtained from Jinan Daigang Biotechnology, China. CCK-8 was purchased from Thermo Fisher Scientific (Waltham, MA, USA). All other chemicals and solvents were of analytical grade.

Preparation of COL/NIC-mPEG-PLGA-NPs

4 mg of colistin was dissolved in 0.2 mL of deionized water to form the inner water phase W_1. 50 mg of mPEG-PLGA and 2 mg of NIC were dissolved in a mixture of 0.8 mL of methylene chloride and acetone (1:1) to form the oil phase O. The inner water phase was mixed with the oil phase and then the mixture is emulsified by ultrasonic treatment for 3 min to form a W_1/O emulsion. Subsequently, 3 mL polyvinyl alcohol aqueous solution (W_2, PVA, 1% w/v) was added, and the mixture was further emulsified by sonication for 5 min to obtain the $W_1/O/W_2$ emulsion. The resulting water-in-oil-in-water (W/O/W) emulsion was slowly dropped into PVA (0.5% w/v) and stirred for 10 min at room temperature. After vacuum evaporation of the solvent, the nanoparticles were collected by centrifugation at room temperature (10000 r/min, 10 min, 3 times) and redispersed in deionized water, followed by vacuum freeze-drying to form a freeze-dried powder of nanoparticles.

Box–Behnken response surface method

Through single-factor experiments, three significant factors affecting the encapsulation efficiency and particle size of COL/NIC-mPEG-PLGA-NPs were screened, namely mPEG-PLGA concentration (X_1), the volume ratio of dichloromethane to acetone (X_2), and PVA concentration (X_3). Meanwhile, the niclosamide encapsulation efficiency (Y_1), colistin encapsulation efficiency (Y_2), and particle size (Y_3) were set as response values. We conducted the optimization design using the Box–Behnken method combined with DesignExpert 13.0 software (Table 1).

Lyophilisation of the nanoparticles

The process of freeze-drying was to remove the water and residual organic solvent from the nanoparticle samples by sublimation and desorption under vacuum. In this study, 5% sucrose, glucose, lactose, and mannitol were added to the nanoparticles, respectively. The nanoparticles were cooled to −60 °C and maintained at the temperature for 12 h. Then the products were transferred to a vacuum freeze dryer and freeze-dried at 0.105 mbar and −50 °C for 48 h.

Characterization

The particle size, PDI, and Zeta potential were observed using dynamic light scattering (Zeta Sizer Nano series Nano-ZSE, Malvern, UK). Each sample was measured three times at 25 °C. The morphology of COL/NIC-mPEG-PLGA-NPs was confirmed using a TEM (JEM-2100C, Jeol Ltd., Japan) after negative staining with sodium phosphotungstate solution (2%, w/w). A Cary 610/670 micro-infrared spectrometer (Agilent Technologies Ltd., Santa Clara, CA) was used to scan in the wave number range of 4000–400 cm^{-1} to obtain the infrared spectra of each sample. COL/NIC-mPEG-PLGA-NPs freeze-dried powder was placed at 4 °C, and samples were taken at 1, 7, 15, 30, and 60 d for the determination of particle size and PDI. The stability study of nanoparticles was also performed by measuring particle size and Zeta potential in water, PBS, FaSSGF, and FaSSIF at predetermined time points at 37 °C for 3 days. For the determination of loading capacity and encapsulation efficiency of colistin and niclosamide, the nanoparticles were placed into a mixed solvent of dichloromethane and methanol (at a volume ratio of 2:1 for dichloromethane to methanol) within an ultrasonic bath to induce demulsification. The quantification of colistin was carried out by means of equal-absorbance dual-wavelength ultraviolet spectrophotometry, while the quantification of niclosamide was achieved through UV-vis spectrometry. Each experiment was repeated three times. The loading capacity (LC) and encapsulation efficiency (EE) of the NPs were calculated by the following equations.

$$\text{Loading capacity (LC)} = \frac{\text{Weight of drug in nanoparticle}}{\text{Weight of feeding polymer and drug}} \times 100\%$$

$$\text{Encapsulation efficiency (EE)} = \frac{\text{Weight of drug in nanoparticle}}{\text{Weight of drug feeded}} \times 100\%$$

The sustained release behavior of COL and NIC from COL/NIC-mPEG-PLGA-NPs was studied by dialysis method. 30 mg of COL/NIC-mPEG-PLGA-NPs freeze-dried powder was dispersed in 5 mL deionized water and then enclosed in dialysis bags (molecular weight cutoff: 3500 Da).

Table 1 | Box–Behnken factor level table

Factor	Level and scope		
	−1	0	1
mPEG-PLGA concentration (X_1)/%	4	5	6
Volume ratio of dichloromethane to acetone (X_2)/v:v	0.5	1	1.5
PVA concentration (X_3)/%	0.5	1	1.5

The dialysis bag was placed in a phosphate buffer solution (PBS, pH 7.4), and then the bag was stirred by a shaker at a constant temperature and a speed of 100 rpm. At predetermined time intervals, 1 mL of the release medium was replaced with 1 mL of fresh release medium. The concentrations of released COL and NIC were determined by visible-UV spectrophotometer, as described above.

Antimicrobial property of COL/NIC-mPEG-PLGA-NPs

MIC of COL/NIC-mPEG-PLGA-NPs was determined using the broth microdilution method[32]. Time–kill curves of the bacteria were performed in duplicate. *E. coli* Y150 culture grown overnight was diluted in LB to OD_{600} = 1.00 followed by a further 1:100 dilution in fresh MHB. Bacteria were then treated with COL/NIC-mPEG-PLGA-NPs (128 μg/mL containing colistin and niclosamide at 1.25 and 0.48 μg/mL, respectively), blank nanoparticles (blank-NPs, 128 μg/mL), free colistin (COL; 1.25 μg/mL), free niclosamide (NIC; 0.48 μg/mL), and mixture of colistin and niclosamide (COL + NIC; 1.25 and 0.48 μg/mL, respectively). At the time points 0, 2, 4, 8, 12, and 24 h, 100 μL aliquots were obtained from each tube, resuspended in PBS, and serially diluted. Subsequently, the dilutions were spotted on LB agar plates and were incubated for 24 h at 37 °C, and after colony counts, the $\log_{10}$ (CFU/mL) of viable cells was determined.

Antibacterial activity was further verified using the LIVE/DEAD bacterial viability kit, where DAPI (blue) is a fluorescent nucleic acid dye that stains all bacterial cells and PI dye (red) only stains bacterial cells with membrane damage[33]. Log phase *E. coli* Y150 bacterial suspension was inoculated 1:10 in fresh LB broth with COL/NIC-mPEG-PLGA-NPs (128 μg/mL containing colistin and niclosamide at 1.25 and 0.48 μg/mL, respectively), blank nanoparticles (blank-NPs, 128 μg/mL), free colistin (COL; 1.25 μg/mL), free niclosamide (NIC; 0.48 μg/mL), and mixture of colistin and niclosamide (COL + NIC; 1.25 and 0.48 μg/mL, respectively), respectively. After growth for 3 h at 37 °C in the shaking incubator, the bacteria were collected by centrifugation, stained with propidium iodide (PI, 10 μg/mL) for 15 min, counterstained with 4′-6-diamidino-2-phenylindole (DAPI, 10 μg/mL) for 5 min in the dark, and then imaged using an inverted fluorescence microscope (EVOS M5000).

The morphology of bacteria was examined using SEM (Zeiss, Germany). *E. coli* Y150 cells were incubated with COL/NIC-mPEG-PLGA-NPs, blank-NPs, COL, NIC, and COL + NIC at 37 °C under the same conditions as above for 1 h, washed, and fixed overnight with 2.5% glutaraldehyde, followed by dehydration with a series of graded ethanol solutions (30, 50, 70, 90, and 100%). The processed samples were dried using a critical point dryer and coated with a layer of gold-palladium using an ion sprayer, and finally observed with SEM (Environmental Scanning Electron Microscope Q45).

Fluorescence assay

Pretreatments of biochemical assays were performed using the following protocols as follows. The tested strain (*E. coli Y*150) was grown overnight at 37 °C with shaking at 200 r/min. Then the cultures were washed and suspended in 5 mM HEPES (pH 7.0, plus 5 mM glucose). In the same buffer, the bacterial suspension's absorbance at OD_{600} was standardized to 0.5, and the fluorescent dye was added. After incubation at 37 °C for 30 min, an aliquot of 1 ml of bacterial suspension was mixed with COL/NIC-mPEG-PLGA-NPs, blank-NPs, COL, NIC, and COL + NIC at the same concentration as mentioned above. After incubation for 1 h, 200 μL bacterial suspension was added to the white 96-well plate with a flat bottom. Subsequently, fluorescence intensity or luminescence was measured by a microplate reader (Tecan Spark 10).

Bacterial cells were washed and resuspended to obtain an OD_{600} of 0.5 with 5 mM HEPES. 1-N-Phenyl-naphthylamine (NPN) (10 μM) assay was used to assess the outer membrane permeability according to a previous study[34]. After 8 min, COL/NIC-mPEG-PLGA-NPs (128 μg/mL containing colistin and niclosamide at 1.25 and 0.48 μg/mL, respectively), blank nanoparticles (blank-NPs, 128 μg/mL), free colistin (COL; 1.25 μg/mL), free niclosamide (NIC; 0.48 μg/mL), and the mixture of colistin and niclosamide (COL + NIC; 1.25 and 0.48 μg/mL, respectively) were injected. Fluorescence intensity of *E. coli* Y150 in the presence of various drugs was measured with excitation wavelength at 350 nm and emission wavelength at 420 nm with an interval of 2 min for 20 min.

3,3-dipropylthiadicarbocyanine iodide ($DiSC_3(5)$, 0.5 μM) was applied to determine the membrane potential[35]. Dissipated membrane potential of *E. coli* Y150 was measured with the excitation wavelength of 622 nm and emission wavelength of 670 nm.

To study the effect of niclosamide on the inhibition of efflux pump, an EtBr efflux assay was performed based on a previous study[36]. The accumulation of EtBr in the cells was monitored with the excitation wavelength at 530 nm and emission wavelength at 600 nm.

Intracellular ATP levels of tested strains were determined using an Enhanced ATP Assay Kit (Beyotime, China). The luminescence of the supernatant was monitored using the Spark 10 M Microplate reader (Tecan). The intracellular ATP levels of the tested strains were calculated based on the luminescence signals.

2′,7′-dichlorodihydrofluorescein diacetate (DCFH-DA, 10 μM) was applied to monitor levels of ROS in *E. coli* Y150[37], following the manufacturer's instruction (Beyotime). Fluorescence intensity was measured with the excitation wavelength of 488 nm and emission wavelength of 525 nm. In addition, H_2O_2 levels of tested strains were determined using a Hydrogen Peroxide Assay Kit (Beyotime, China). After incubation for one hour, the absorbance of lysis buffer at 560 nm was measured.

L-Ascorbic acid, an antioxidant as ROS quencher (L-Aa, 10 mM), was used to determine the impact of ROS on the antibacterial efficacy of COL/NIC-mPEG-PLGA-NPs[38].

In vitro and in vivo biocompatibility of COL/NIC-mPEG-PLGA-NPs

We evaluated the blood compatibility of COL/NIC-mPEG-PLGA-NPs by hemolysis assay[39]. We collected mouse red blood cells by centrifuging the blood. We diluted COL/NIC-mPEG-PLGA-NPs to different concentrations (512, 256, 128, 64, 32, and 16 μg/mL) and incubated them with red blood cell suspensions at 37 °C for 3 h. We measured the optical density of the sample at 540 nm (OD_{540} nm) using an enzyme labeler (Tecan Spark 10 M). The cytotoxicity of COL/NIC-mPEG-PLGA-NPs was evaluated by CCK-8 assay. The PK-15 cells and murine macrophage cell line RAW 264.7 was inoculated in 96-well plates at a density of 5000 cells per well and cultured at 37 °C and 5% CO_2. When the cells reached about 70% confluent, each well was treated with the medium containing different concentrations of COL/NIC-mPEG-PLGA-NPs (1000, 500, 250, 125, 62.5, and 31.25 μg/mL), and cells cultured in blank media were used as controls. After incubation for 24 h, the cells were treated with 10 μL CCK8 and 90 μL blank medium. Last, the viability of PK-15 cells and RAW 264.7 cells were measured by recording and calculating according to the absorbance at 450 nm through a microplate reader, respectively. To evaluate the in vivo biocompatibility, BALB/c mice (6 to 8 weeks) were randomly divided into three groups (n = 4) and treated with COL/NIC-mPEG-PLGA-NPs (L) (20 mg/kg), COL/NIC-mPEG-PLGA-NPs (M) (40 mg/kg), or COL (10 mg/kg) via intraperitoneal injection, respectively. After two days, the sera were collected for biochemical analysis including alkaline phosphatase (ALT), aspartate aminotransferase (AST), urea nitrogen (BUN), and creatinine (CREA) to evaluate the functions of the liver and kidney[40].

Targeting effect in vivo

In vivo biodistribution of COL/NIC-mPEG-PLGA-NPs: The biodistribution of COL/NIC-mPEG-PLGA-NPs was evaluated in vivo using mice (n = 8). After injecting the mice intravenously (i.v.) with DiR-COL/NIC-mPEG-PLGA-NPs (100 μL/mouse), the mice were imaged using IVIS (λex/λem = 748/780 nm) at predetermined time points (0, 1, 3, 6, 9, 12, 24, and 48 h).

In vivo Targeted Imaging of Bacterial Infections: A muscle infection model was employed to evaluate the in vivo targeting ability of COL/NIC-mPEG-PLGA-NPs. Mice (n = 10) were intramuscularly injected with PBS

(100 μL) and *E. coli* (1.2×10^8 CFU/mouse, 100 μL) into the left and right thighs respectively (i.e., the uninfected site and the infected site). After 24 h, the mice were intravenously injected (i.v.) with DiR-COL/NIC-mPEG-PLGA-NPs, and imaged by IVIS at predetermined time points (1, 3, 6, 9, 12, and 24 h). After 24 hours of treatment, the mice were sacrificed for ex vivo imaging. The major organs (heart, liver, spleen, lungs, kidneys, both legs) were collected and imaged using IVIS.

Antibacterial efficacy of COL/NIC-mPEG-PLGA-NPs in vivo

To evaluate the in vivo therapeutic efficacy of COL/NIC-mPEG-PLGA-NPs, BALB/c mice (6 to 8 weeks) were treated with *E. coli* Y150 (10^8 CFU/20 g, 100 μL) intraperitoneally to establish an acute peritonitis infection model. The infected mice were randomly divided into seven groups ($n = 8$ for each group), and the mice were treated with different drug formulations, including physiological saline (as the untreated control), colistin alone, niclosamide alone, the combination of colistin and niclosamide, and COL/NIC-mPEG-PLGA-NPs at a fixed dose (colistin: 5 mg/kg; niclosamide: 5 mg/kg; COL + NIC: 5 mg/kg + 5 mg/kg; COL/NIC-mPEG-PLGA-NPs: 20 mg/kg (low-dose group), 40 mg/kg (medium-dose group), 80 mg/kg (high-dose group), respectively). Intraperitoneal drug injection was performed after mice were infected with bacteria for 1 h. The health status of mice was monitored over 168 h, and the survival rate was recorded to draw the survival curves.

After the same drug treatment as described in the previous paragraph, blood samples were taken from eyeballs at 24 h postinfection, and the mice were sacrificed and dissected to obtain the peritoneal fluid, liver, spleen, and kidney. The harvested organs were ground into tissue homogenates and continuously diluted with sterile saline. The diluted homogenate (20 μL) was added to LB solid medium, cultured overnight at 37 °C, and colony counting was performed. Each experiment was conducted in triplicate. The results were presented as the mean ± SD ($n = 5$). The mouse organs (liver, spleen, and kidney) in each group were harvested, fixed in 4% paraformaldehyde, dehydrated, and encapsulated in wax blocks. Tissue samples were cut into 3-μm thin slices and stained with H&E for histological analysis.

Ethical statement

All the in vivo experiments were approved by the Administration of Affairs Concerning Experimental Animals of the State Council of the People's Republic of China (approved on 11-14-1988). All animal experiments have been approved by the Animal Care and Use Committee of Henan Agricultural University, and we have adhered to all relevant ethical regulations concerning animal use.

Statistics and reproducibility

Statistical analysis was performed using GraphPad Prism 8, Origin2021, and SPSS software. Each experiment included at least three independent biological replicates. All data are presented as mean ± SD. Unless otherwise noted, unpaired *t*-test between two groups or one-way ANOVA among multiple groups were used to calculate *p*-values ($^*p < 0.05$, $^{**}p < 0.01$, $^{***}p < 0.001$).

Reporting summary

Further information on research design is available in the Nature Portfolio Reporting Summary linked to this article.

Data availability

All data generated or analyzed during this study are included in the published article and Supplementary Information. Source data for the main figures are provided in Supplementary Data 1. And all other data included in this study are available upon request by contact with the corresponding author.

Received: 3 August 2024; Accepted: 16 April 2025;
Published online: 29 April 2025

References

1. LaPlante, K., Cusumano, J. & Tillotson, G. Colistin for the treatment of multidrug-resistant infections. *Lancet Infect. Dis.* **18**, 1174–1175 (2018).
2. Mendelson, M. et al. The One Health stewardship of colistin as an antibiotic of last resort for human health in South Africa. *Lancet Infect. Dis.* **18**, e288–e294 (2018).
3. Liu, Y. Y. et al. Emergence of plasmid-mediated colistin resistance mechanism MCR-1 in animals and human beings in China: a microbiological and molecular biological study. *Lancet Infect Dis* **16**, 161–168 (2016).
4. Choi, Y. et al. Comparison of fitness cost and virulence in chromosome- and plasmid-mediated colistin-resistant Escherichia coli. *Front. Microbiol.* **11**, 798 (2020).
5. Xu, Y. et al. An Evolutionarily conserved mechanism for intrinsic and transferable polymyxin resistance. *mBio* **9**, 2 (2018).
6. Andrade, F. F., Silva, D., Rodrigues, A. & Pina-Vaz, C. Colistin update on its mechanism of action and resistance, present and future challenges. *Microorganisms* **8**, 11 (2020).
7. Hald, T. et al. World health organization estimates of the relative contributions of food to the burden of disease due to selected foodborne hazards: a structured expert elicitation. *PLoS ONE* **11**, e0145839 (2016).
8. Copp, J. N. et al. Mechanistic understanding enables the rational design of salicylanilide combination therapies for gram-negative infections. *mBio* **11**, 5 (2020).
9. Ayerbe-Algaba, R. et al. Synergistic activity of niclosamide in combination with colistin against colistin-susceptible and colistin-resistant acinetobacter baumannii and Klebsiella pneumoniae. *Front. Cell Infect. Microbiol.* **8**, 348 (2018).
10. Domalaon, R., De Silva, P. M., Kumar, A., Zhanel, G. G. & Schweizer, F. The anthelmintic drug niclosamide synergizes with colistin and reverses colistin resistance in gram-negative bacilli. *Antimicrob. Agents Chemother.* **63**, 4 (2019).
11. Zhang, L. X. et al. Niclosamide attenuates inflammatory cytokines via the autophagy pathway leading to improved outcomes in renal ischemia/reperfusion injury. *Mol. Med. Rep.* **16**, 1810–1816 (2017).
12. Sorlí, L. et al. Trough colistin plasma level is an independent risk factor for nephrotoxicity: a prospective observational cohort study. *BMC Infect. Dis.* **13**, 380 (2013).
13. Forrest, A. et al. Pharmacokinetic/toxicodynamic analysis of colistin-associated acute kidney injury in critically Ill patients. *Antimicrob. Agents Chemother.* **61**, 11 (2017).
14. Tran, T. B. et al. Pharmacokinetics/pharmacodynamics of colistin and polymyxin B: are we there yet? *Int. J. Antimicrob. Agents* **48**, 592–597 (2016).
15. Grottkau, B. E., Cai, X., Wang, J., Yang, X. & Lin, Y. Polymeric nanoparticles for a drug delivery system. *Curr. Drug Metab.* **14**, 840–846 (2013).
16. Guo, J. et al. Aptamer-functionalized PEG-PLGA nanoparticles for enhanced anti-glioma drug delivery. *Biomaterials* **32**, 8010–8020 (2011).
17. Danhier, F. et al. PLGA-based nanoparticles: an overview of biomedical applications. *J. Control Release* **161**, 505–522 (2012).
18. Avgoustakis, K. et al. Effect of copolymer composition on the physicochemical characteristics, in vitro stability, and biodistribution of PLGA-mPEG nanoparticles. *Int. J. Pharm.* **259**, 115–127 (2003).
19. Chen, Y., Wang, F. & Benson, H. A. Effect of formulation factors on incorporation of the hydrophilic peptide dalargin into PLGA and mPEG-PLGA nanoparticles. *Biopolymers* **90**, 644–650 (2008).
20. Park, J. et al. PEGylated PLGA nanoparticles for the improved delivery of doxorubicin. *Nanomedicine* **5**, 410–418 (2009).
21. Lin, Y., Zhuang, X., Xie, B. & Chen, H. Enhanced antitumor efficacy of docetaxel-loaded monomethoxy Poly(ethylene glycol)-Poly(D, L-

lactide-co-glycolide) amphiphilic copolymer against non-small cell lung cancer. *J. Nanosci. Nanotechnol.* **20**, 7263–7270 (2020).
22. Pays, K., Giermanska-Kahn, J., Pouligny, B., Bibette, J. & Leal-Calderon, F. Double emulsions: how does release occur? *J. Control Release* **79**, 193–205 (2002).
23. Wang, H. et al. Enhanced anti-tumor efficacy by co-delivery of doxorubicin and paclitaxel with amphiphilic methoxy PEG-PLGA copolymer nanoparticles. *Biomaterials* **32**, 8281–8290 (2011).
24. Mahmoud, B. S. & McConville, C. Box-Behnken design of experiments of polycaprolactone nanoparticles loaded with irinotecan hydrochloride. *Pharmaceutics* **15**, 4 (2023).
25. Wang, L. et al. Cryoprotectant choice and analyses of freeze-drying drug suspension of nanoparticles with functional stabilisers. *J. Microencapsul.* **35**, 241–248 (2018).
26. Wang, Y., Gao, S., Ye, W. H., Yoon, H. S. & Yang, Y. Y. Co-delivery of drugs and DNA from cationic core-shell nanoparticles self-assembled from a biodegradable copolymer. *Nat. Mater.* **5**, 791–796 (2006).
27. Jiang, Y. et al. The interplay of size and surface functionality on the cellular uptake of sub-10 nm gold nanoparticles. *ACS Nano* **9**, 9986–9993 (2015).
28. Karakoti, A. S., Das, S., Thevuthasan, S. & Seal, S. PEGylated inorganic nanoparticles. *Angew. Chem. Int. Ed. Engl.* **50**, 1980–1994 (2011).
29. Hong, Y., Zeng, J., Wang, X., Drlica, K. & Zhao, X. Post-stress bacterial cell death mediated by reactive oxygen species. *Proc. Natl. Acad. Sci. USA* **116**, 10064–10071 (2019).
30. Belenky, P. et al. Bactericidal antibiotics induce toxic metabolic perturbations that lead to cellular damage. *Cell Rep.* **13**, 968–980 (2015).
31. Jafari, F. & Elyasi, S. Prevention of colistin induced nephrotoxicity: a review of preclinical and clinical data. *Expert Rev. Clin. Pharmacol.* **14**, 1113–1131 (2021).
32. Humphries, R., Bobenchik, A. M., Hindler, J. A. & Schuetz, A. N. Overview of changes to the clinical and laboratory standards institute performance standards for antimicrobial susceptibility testing, M100, 31st Edition. *J. Clin. Microbiol.* **59**, e0021321 (2021).
33. Kang, S., Pinault, M., Pfefferle, L. D. & Elimelech, M. Single-walled carbon nanotubes exhibit strong antimicrobial activity. *Langmuir* **23**, 8670–8673 (2007).
34. Song, M. et al. A broad-spectrum antibiotic adjuvant reverses multidrug-resistant Gram-negative pathogens. *Nat. Microbiol.* **5**, 1040–1050 (2020).
35. Hamamoto, H. et al. Lysocin E is a new antibiotic that targets menaquinone in the bacterial membrane. *Nat. Chem. Biol.* **11**, 127–133 (2015).
36. Yi, K. et al. Synergistic antibacterial activity of tetrandrine combined with colistin against MCR-mediated colistin-resistant Salmonella. *Biomed. Pharmacother.* **149**, 112873 (2022).
37. Liu, Y. et al. Metformin restores tetracyclines susceptibility against multidrug resistant bacteria. *Adv. Sci. (Weinh)* **7**, 1902227 (2020).
38. Zhao, H. et al. Antibiotic-polymer self-assembled nanocomplex to reverse phenotypic resistance of bacteria toward last-resort antibiotic colistin. *ACS Nano* **17**, 15411–15423 (2023).
39. Neun, B. W. & Dobrovolskaia, M. A. Method for analysis of nanoparticle hemolytic properties in vitro. *Methods Mol. Biol.* **697**, 215–224 (2011).
40. Tang, Q. et al. Hydrophobic modification improves the delivery of cell-penetrating peptides to eliminate intracellular pathogens in animals. *Acta Biomater.* **157**, 210–224 (2023).

Acknowledgements

This work was supported by the National Key Research and Development Program of China (2023YFD1800105), the National Natural Science Foundation of China (32102716), and the National Natural Science Foundation of China (32373069).

Author contributions

Y.J.Z. and G.Z.H. designed this project; K.F.Y., P.L.L., and X.L.W. performed experiments and drafted this manuscript. Y.L.G. and D.D.H helped with checkerboard and time-kill analysis; Y.S.P. and X.Y.M helped with animal experiments; G.Z.H. designed the experiments, supervised the project, and wrote the manuscript.

Competing interests

The authors declare no competing interests.

Additional information

Supplementary information The online version contains supplementary material available at https://doi.org/10.1038/s42003-025-08095-8.

Correspondence and requests for materials should be addressed to Gongzheng Hu or Yajun Zhai.

Peer review information *Communications Biology* thanks the anonymous reviewers for their contribution to the peer review of this work. Primary Handling Editors: Dr Dr Periklis Pantazis and Dr Ophelia Bu. A peer review file is available.